

Enhanced Optical Emission During Crab Giant Radio Pulses

A. Shearer^{1*}, B. Stappers^{2,3}, P. O' Connor¹, A. Golden¹,
R. Strom^{2,3}, M. Redfern¹ & O. Ryan¹

¹National University of Ireland, Galway,
Newcastle Rd., Galway, Ireland

²Stichting ASTRON, 7990 AA Dwingeloo, The Netherlands

³Sterrenkundig Instituut "Anton Pannekoek",
1098 SJ Amsterdam, The Netherlands

*To whom correspondence should be addressed; E-mail: andy.shearer@nuigalway.ie

We detected a correlation between optical and giant radio pulse emission from the Crab pulsar. Optical pulses coincident with the giant radio pulses were on average 3% brighter than those coincident with normal radio pulses. Combined with the lack of any other pulse profile changes, this result indicates that both the giant radio pulses and the increased optical emission are linked to an increase in the electron-positron plasma density.

Despite more than 30 years of observation the emission mechanism of pulsars is still a matter of debate (1). A broad consensus does exist: that luminosity is powered by the rotation of the pulsar, that the pulsed radio signal comes from a coherent process, and that the optical-to-X-ray emission is incoherent synchrotron radiation whereas the γ -ray emission is curvature radiation (2). What is not agreed on is the mechanism that accelerates the electrons to the energy required for synchrotron and curvature radiation, where this acceleration takes place,

how coherency is maintained, and the stability of the electron-positron plasma outflow from the neutron star's surface (3, 4). From the radio-pulse profile at 1380 MHz and the optical profile for the Crab pulsar (Fig. 1), we can identify two primary features: a main pulse and an inter-pulse. At lower energies a radio precursor can be seen and at higher energies in the optical, x-ray and γ -ray regions, bridge emission can be seen between the main pulse and the interpulse. One suggestion is that the precursor represents emission from the pulsar polar cap region near the neutron star surface, similar to the radio emission from most pulsars, and that the other features come from higher in the magnetosphere (5). On a pulse-by-pulse basis, the radio emission is chaotic, whereas over a prolonged period the average radio pulse profile is steady. This picture is made more complex by the existence of giant radio pulses (GRPs) that occur at random intervals, in phase with either the main pulse or interpulse (Fig. 1), and that have energies about 1000 times as high as than the mean energy (6). In the optical and infrared energy regions the pulse profile is constant at the 1% level (7, 8).

The Crab pulsar was first detected through its GRP component (9). Since then, only three other pulsars have shown similar behaviour. Two of the others are recycled millisecond pulsars - PSR B1937+21 (10) and PSR B1821-24 (11) - of which the latter is in a globular cluster. In comparison with the Crab pulsar they are much older and have surface magnetic fields some 1/10,000th as strong. The third, which has been reported only recently, is PSR B0540-69 (12) - a pulsar similar to the Crab pulsar in the large Magellanic Cloud. The only feature that seems to link these pulsars is the magnetic field strength at the light cylinder (13, 11). To investigate this possibility and to examine other aspects of GRP emission, and hence radio emission in general, we would need to see whether the GRP phenomena can be seen at other energies. Any observed variation in the emitted flux, pulse morphology, or phase relations at higher energies coincident with a GRP would provide explicit constraints on pulsar (coherent/incoherent) emission physics and geometry. A previous study (6) searched for correlations between low-energy γ ray emis-

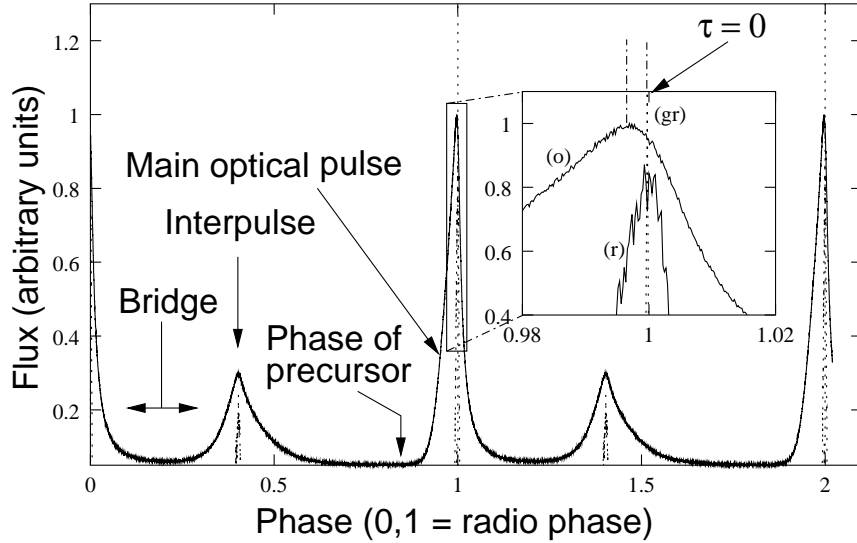


Figure 1: The Crab pulse profile showing the optical light curve(o), the average radio light curve at 1380 MHz(r) and a single giant pulse at 1357.5MHz (gr). τ , time. Two periods are shown for clarity. Various pulse parameters have been identified. Also shown is the location of the precursor observed at lower frequencies and the bridge emission seen particularly at higher frequencies. On this scale, the GRP width corresponds to ≈ 0.00035 units of phase (12 μ s), the radio pulse to ≈ 0.009 (300 μ s), and the optical pulse to ≈ 0.045 (1500 μ s). The optical light curve is taken from the second night of observation. The avalanche photodiode (APD) bandpass for these observations was from 6000 to 7500Å. Phase 0 corresponds to the arrival at the solar system barycentre of the peak radio pulse. The optical light curve for this plot was divided into 5000 phase bins; the optical peak is at -100 μ s with respect to the JBE.

sion and GRPs. Those investigators measured a γ -ray giant pulse upper limit of 2.5 times the average flux and found that no other γ -ray pulse parameters (width, arrival time, or spectrum) varied during GRP events. They estimated that 60% of the upper limit could be due to inverse Compton scattering of the radio photons on the local plasma.

To investigate whether there is a link between the radio and optical emission from the Crab pulsar, we made simultaneous observations with the Westerbork Synthesis Radio Telescope (WSRT) and with the Transputer Instrument for Fast Image Detection (TRIFFID) optical photometer (14) mounted on the 4.2 m William Herschel Telescope (WHT) (Table 1). The radio observations were made at a central frequency of 1357.5 MHz with the WSRT in tied-array

Date	Start time (UTC)		Duration (seconds)	
	Optical	Radio	Optical	Radio
2 November 1999	23:29:39	23:30:00	6500.0	5400.0
3 November 1999	23:30:00	23:37:20	5320.0	6000.0

Table 1: Summary of the radio and optical observations

mode - making it equivalent to a 94-m dish - and the pulsar signal analyser PuMa (pulsar machine)(15)). A 5 MHz band was Nyquist sampled and coherently dedispersed (16, 17) at a dispersion measure of $56.791 \text{ cm}^{-3} \text{ pc}$. Samples were then combined to produce a time series with a resolution of $6.4 \mu\text{s}$. This time series was searched for signal-to-noise peaks greater than 10σ , equivalent to a flux density of 150 jansky (Jy) and ~ 1000 times as strong as the normal radio emission (18). All 10,034 peaks were located at pulse longitudes corresponding to the main pulse and the interpulse, as defined by the average radio emission, thereby identifying them as GRPs. The energy of the GRPs was subsequently calculated by summing together all significant samples within $\pm 1.5 \text{ ms}$ and using the same flux scale given above for the peaks. The amplitude distribution of the GRPs showed the expected functional form (Fig. S1) (6). Conditions on the second night of optical observations were good: Seeing was better than $1''$ for the duration of the observations, and the transparency varied by less than 20%. On the first night, sky transparency was poor ($< 50\%$ of the first night and variable) and the seeing was $1.5''$.

Time alignment of the optical and radio data was achieved with the Jodrell Bank Crab pulsar ephemeris (JBE, (19)) appropriate for November 1999 (Table 2) and the optical and radio arrival times were transformed to the solar system barycentre with the DE200 Jet Propulsion Laboratory (JPL) ephemeris (20). These data were then folded in phase with the JBE to determine the relative phase with respect to the radio emission of each optical photon and each GRP. After alignment, we found that the average GRP arrival time is $9.5 \mu\text{s}$ before that predicted by

the JBE, well within the $19\ \mu\text{s}$ error in this ephemeris. The average optical pulse arrived $100 \pm 20\ \mu\text{s}$ before the JBE prediction (Fig 1). Those GRPs coincident with the interpulse were coincident with the peak of the optical interpulse to within the fitting error of $10\mu\text{s}$.

Jodrell Bank Ephemeris valid from MJD 51467.85318 to MJD 51504.74933			
Pulse arrival time	1999/11/02 00:00:00.026917 ± 0.000019		UT
Modified Julian Date	51484.00000031154	± 0.00000000023	days
Period	0.033502974639313	± 0.00000000000192	s
Pulsar Frequency	29.848095900910629	± 0.000000000170673	Hz
Frequency 1st derivative	-374639.721220770	± 0.358888933	10^{-15}s^{-2}
Frequency 2nd derivative	10302.350019155		10^{-24}s^{-3}
First Pulse Arrival Time (MJD)			
	Optical		Radio
1999, November 2 :	51484.98377619		51484.98404246
1999, November 3 :	51485.98408505		51485.98917482

Table 2: Ephemeris and pulse arrival times.

Because the optical data were subject to fluctuations in sky transparency (on a timescale of ≈ 30 s), only the photons that were detected 20 periods before and after the GRP and during the GRP itself, were used for subsequent study. This resulted in a total of 10,034 data sets of 41 periods each. Folding the optical photons at the Crab's period and then averaging over all data sets (but not including the period associated with a GRP) we form an average pulse profile (Fig 2). For comparison we also show the pulse profile formed by averaging only the optical pulses coincident with a GRP. This profile shows that the giant optical pulses are on average 3% brighter than normal optical pulses (although there is no statistical difference in the location or sharpness of the peak). We found that the optical pulses coincident with the GRPs were $7.8\ \sigma$ brighter than the mean profile (Fig. S2).

We also analyzed other pulse parameters: arrival time, pulse shape, and interpulse height. None of these parameters showed any statistically significant variation with the presence of a

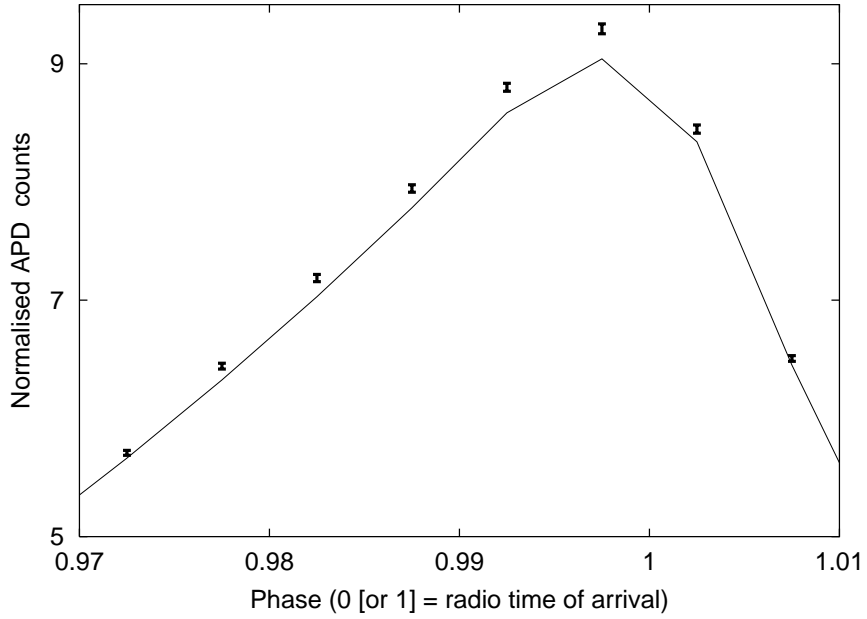


Figure 2: The mean optical ‘giant’ pulse superimposed (with its error bars) on the average optical pulse. The average pulse is determined from the 40 pulsar periods centred on the GRP, but not including it, from both nights of observation.

GRP (Fig. S3). The arrival time for the optical giant pulses was on average the same as the optical pulses coincident with non-GRPs, to within $20 \mu\text{s}$ (Fig 2). The pulse widths for the same pulses were similar at the 10% level (Fig. S4). All the individual optical pulse profiles are scaled down versions of the average optical pulse profile - in contrast to the radio pulses.

Some 15% of the GRPs were coincident in phase with the interpulse. However, there was no noticeable effect on the optical interpulse height, giving a 1σ upper limit of 2.5%. There was, however, a small effect on the optical main pulse, albeit at low significance, an increase of 2% (1.75σ). The optical interpulse showed no change in amplitude during a GRP associated with the main pulse. There was a slight increase in the significance of the main peak variation when only the midrange GRPs were chosen (Fig 3). To convert the quoted fluxes to luminosity, it would be necessary to account for possible differences between the radio and optical beaming fractions (21). From these observations, we have established a link between optical and radio

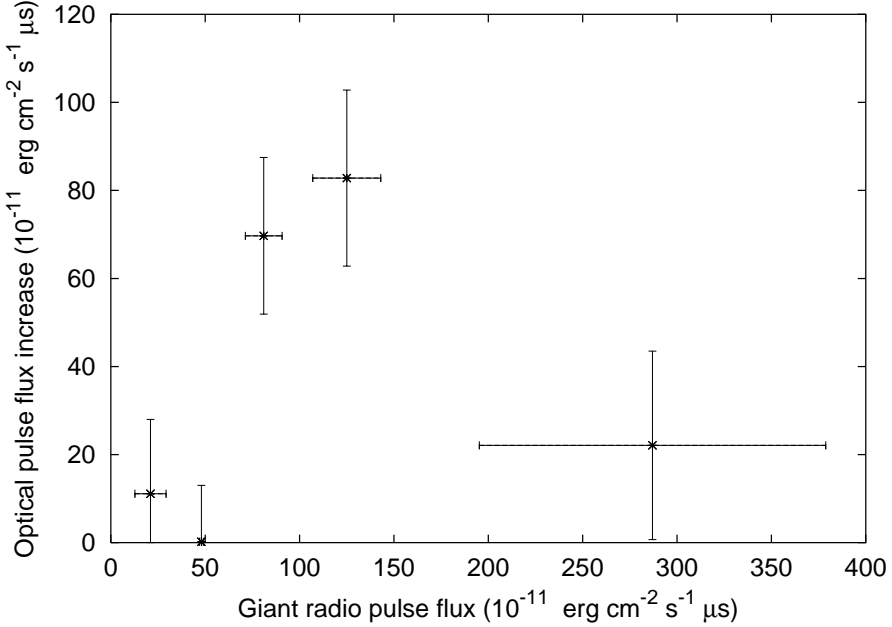


Figure 3: The link between optical pulse size and GRP energy for the second night of observation. The plot shows the increase in the optical pulse flux against the GRP flux. The data have been binned using the radio flux, with approximately equal events in each bin. We calculated the optical pulse flux assuming that the main peak has an average flux of 1.9 mJy, (26) and integrating from 0.9 to 1.05 in phase. The radio flux was calculated by determining excess counts above noise for ± 0.1 periods around a detected GRP, then converting these counts to janskys.

flux variations. The fact that only the optical pulse, which is coincident with a GRP, shows enhanced intensity suggests that the coherent (radio) and incoherent (optical) emissions produced in the Crab pulsar's magnetosphere are linked.

Among a number of mechanisms that might explain the radio-optical connection, several would appear to be unlikely. A decrease in the opacity affecting the optical luminosity is probably ruled out by the expected viewing geometry, because the light does not necessarily pass through the radio emission region. A change in the geometry of the optical emission region induced by the GRP mechanism is not likely, because we see no change in optical pulse shape or phase. In particular, we do not expect the path over which the optical radiation is emitted to have changed. Increases in magnetic field strength (leading to enhanced optical emission) can prob-

ably be ruled out on a global scale; local magnetic field enhancements due to increased plasma density might occur, but they are probably insufficient to explain the observations. Inverse-Compton scattering of the GRP photons, kicking them up to the optical band, seems unlikely on several grounds, because only about 1% of the radio energy should appear as optical emission (22), whereas we find nearly equal luminosities. The γ -ray upper limit (6) also suggests no more than $\simeq 1\%$ conversion.

A consistent explanation is that the optical emission is a reflection of increased plasma density that causes the GRP event. Whatever triggers the GRP phenomenon, it releases energy uniformly throughout most of the electromagnetic spectrum, as implied by the similar energies of radio and enhanced optical pulses. Changes in the pair production rate at the level of a few percent could explain the optical variations and would also be expected at higher energies; existing limits to enhanced γ -ray emission (6) do not contradict this. However, an additional mechanism would be needed to account for the radio GRPs, which are orders of magnitude stronger than the average pulse level. It has been suggested (22) that this could be achieved by local density enhancements to the plasma stream, which increase the coherent emission ($\propto n^2$) with little effect on the (high-energy) incoherent radiation($\propto n$). These changes must occur on tiny timescales ($< 10\mu\text{s}$) to explain the observed change in optical flux and the upper limit in the γ -ray region (6, 23). This result is also consistent with the recent observations of nanosecond timescale structure within GRPs, (24). Whatever the mechanism, our observations demonstrate a clear link at the individual pulse level between the coherent and incoherent emission regimes in the Crab pulsar.

References and Notes

1. M. Lyutikov, R. D. Blandford, G. Machabeli, *Mon Not R. Astron. Soc.*, **305**, 338L (1999)

2. Synchrotron and curvature radiation are produced when a charged particle moves in the vicinity of a magnetic field. Synchrotron radiation is produced when the particle follows a gyratory path around a magnetic field line and curvature radiation is the limit when the particle follows a curved field line. See (25) for a detailed treatment.
3. A. K. Harding and J. K. Daugherty, *Adv. Space Res.* **21**, 251H (1998)
4. R. W. Romani, *Astrophys. J.* **470**, 469 (1996)
5. R. W. Romani and I.-A. Yadigaroglu, *Astrophys. J.* **438**, 314 (1995)
6. S. C. Lundgren, *et al*, *Astrophys. J.* **453**, 433 (1995)
7. D. Hegyi, R. Novick and P. Thaddeus, *IAU Symposium*, **46**, 129 (1971)
8. D. H. P. Jones, F. G. Smith and J. E. Nelson, *Nature*, **283**, 50 (1980)
9. D. H. Staelin and E. C. Reifenstein, *Science*, **162**, 1481 (1968)
10. I. Cognard, J. A. Shrauner, J. H. Taylor and S. E. Thorsett, *Astrophys. J.* **457**, L816 (1996)
11. R. W. Romani and S. Johnston, *Astrophys. J.* **557**, L93 (2001)
12. S. Johnston and R. W. Romani, *Astrophys. J.* **590**, L95 (2003); available at <http://arxiv.org/abs/astro-ph/0305235>
13. The light cylinder is defined as the distance at which the co-rotation velocity equals the speed of light.
14. D. Buckton, O. Ryan, A. Shearer, R. Redfern, R.F. Butler, *Proc. SPIE*, **4876**, in press.
15. J. L. L. Voûte *et al*, *Astron. Astrophys.* **385**, 733 (2002)
16. T. H. Hankins, *Astrophys. J.* **169**, 487 (1971)

17. Radio propagation through the interstellar medium is subject to a frequency-dependent delay that is proportional to the line-of-sight electron density. This delay can be completely corrected for by with the appropriate filter, and in that case it is referred to as coherent dedispersion.
18. The width of the WSRT tied-array fan beam is ~ 10 arcseconds and the total contribution of the Crab nebula emission to the system temperature is ~ 120 K.
19. M. Roberts, personal communication
20. E. M. Standish, *Astron. Astrophys.* **114**, 297 (1982)
21. The beaming fraction describes what fraction of the sky is illuminated by the pulsar during each rotation. It is a reasonable assumption that this fraction will be energy dependent.
22. R. D. Blandford and E. T. Scharlemann, *Mon. Not. R. Astron. Soc.*, **174**, 59(1976)
23. J. Arons, *Space Sci. Rev.* **24**, 437 (1970)
24. T. H. Hankins, J. S. Kern, J. C. Weatherall and J. A. Eilek, *Nature*, **422**, 141 (2003)
25. G. F. Rybicki, and A. P. Lightman, *Radiative Processes in Astrophysics* (Cambridge University Press, Cambridge, UK, 1979)
26. A. Golden *et al*, *Astron. Astrophys.* **363**, 617 (2000)
27. We thank Enterprise Ireland is thanked for its support under the Basic Grant Research scheme. P.O.C. is grateful for support under the HEA funded CosmoGrid project. The WHT is operated on the island of La Palma by the Isaac Newton Group in the Spanish Observatorio del Roque de los Muchachos of the Instituto de Astrofisica de Canarias. The WSRT is operated by ASTRON with financial support from the Netherlands Organisation

for Scientific Research (NWO). We thank M. Roberts from Jodrell Bank for the provision of the radio ephemeris(JBE), R. Butler for help in the production of this manuscript and A. Boyle for her help during the optical observations.

Supporting Online Material

www.sciencemag.org/cgi/content/full/301/5632/493/DC1

Figs. S1 to S4

Accepted 18 June 2003